Geochemical Perspectives Letters

Isotopic fractionation of neon during magma degassing

E. Núñez-Guerrero[1*], M. Moreira[1], B. Scaillet[1]

OPEN ACCESS

https://doi.org/10.7185/geochemlet.2505

Abstract

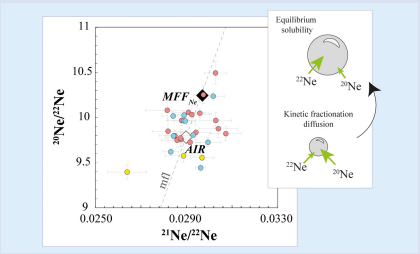

Determining the neon isotope composition of the Earth's mantle is key to unravelling how light noble gases became part of the primordial Earth. However, accurately measuring neon abundance and isotopic composition in primary mantle melts is challenging due to the low concentration of neon, coupled with potential isotopic fractionation during transport and degassing. Interestingly, natural samples that exhibit solar-like neon isotopic compositions, ranging between the values calculated for the Sun ($^{20}Ne/^{22}Ne = 13.36 \pm 0.09$; Heber *et al.*, 2012) and those resulting from solar wind implantation and sputtering ($^{20}Ne/^{22}Ne = 12.73$; Moreira and Charnoz, 2016), support the idea that the Earth's mantle might have trapped a primordial nebula in its early formation stages. Analyses of three synthetic vesiculated glasses, produced at ~1.7 kbar and 1200 °C using a starting material with an air-like isotopic composition ($^{20}Ne/^{22}Ne = 9.81$ and $^{21}Ne/^{22}Ne = 0.0287$) fluxed with CO_2, reveal significant isotopic fractionation of Ne within trapped vesicles. Measured values reach $^{20}Ne/^{22}Ne = 10.50 \pm 0.14$. The isotopic variations among individual vesicles align with expectations for kinetic fractionation, suggesting that degassing processes affect Ne isotope composition of basaltic melts.

Received 21 June 2024 | Accepted 13 January 2025 | Published 10 February 2025

Introduction

Determining the neon isotopic ratio of the Earth's mantle is fundamental to understanding the mechanism of incorporation of the noble gases in the primordial Earth. Two main models have been proposed to explain the origin of neon in the mantle: (i) solar nebula gas dissolution, and (ii) accretion of solar wind-irradiated material. The first model posits that neon was incorporated into a magma ocean after gravitational capture of a dense primary H_2-He atmosphere (Mizuno *et al.*, 1980; Harper Jr and Jacobsen, 1996; Yokochi and Marty, 2004; Mukhopadhyay, 2012; Williams and Mukhopadhyay, 2019). The second model proposes that neon was acquired before Earth's accretion on dust irradiated by the early Sun, in the inner solar system (Trieloff *et al.*, 2000; Ballentine *et al.*, 2005; Raquin and Moreira, 2009; Kurz *et al.*, 2009; Colin *et al.*, 2015; Moreira and Charnoz, 2016; Péron *et al.*, 2016, 2017, 2018). However, distinguishing between the solar nebula component and the implanted solar wind is challenging due to the similarity of their $^{20}Ne/^{22}Ne$ isotopic compositions; 13.36 ± 0.16 for the outer convective zone of the Sun and 12.52 – 12.75 for steady state composition of the solar wind (Black, 1972; Eberhardt *et al.*, 1972; Raquin and Moreira, 2009; Heber *et al.*, 2012; Moreira and Charnoz, 2016).

In terms of the isotopic composition of the light noble gases, particularly neon, the long term degassing process of the mantle results in differences in concentrations and isotopic compositions between Oceanic Island Basalts and Mid-Ocean Ridge basalts (OIBs and MORBs respectively). In the mantle, the production of ^{20}Ne and ^{22}Ne is negligible (Yatsevich and Honda, 1997), and thus the $^{20}Ne/^{22}Ne$ isotopic ratio can be considered to record the composition of primordial neon in the Earth's mantle. The lower mantle has undergone less degassing and retains higher concentrations of primordial noble gases, indicating the presence of an ancient, primordial composition. (Honda *et al.*, 1993; Moreira *et al.*, 1998; Ballentine *et al.*, 2005; Mukhopadhyay, 2012; Péron *et al.*, 2017; Trieloff *et al.*, 2000). Unlike MORB sources, plume sources exhibit different trends for the neon isotopic composition as seen, for instance, in the Galapagos plume, which is considered as one of the most primitive neon sources in terms of the nucleogenic neon isotopic composition ($^{21}Ne/^{22}Ne = 0.0345 \pm 0.0004$), with a $^{20}Ne/^{22}Ne$ isotopic ratio estimated to be 12.65 ± 0.04 (2σ) (Péron *et al.*, 2017). Values of $^{20}Ne/^{22}Ne$ higher than 12.65 are sometimes observed (*e.g.*, the South Atlantic, Iceland, and Kola Peninsula of Russia; Yokochi and Marty, 2004; Mukhopadhyay, 2012; Williams and Mukhopadhyay, 2019), which was interpreted as reflecting a mantle source having a neon composition similar to the solar nebula.

Step crushing is commonly used for the analysis of noble gases trapped in vesicles of basaltic glass during magma degassing (*e.g.*, Moreira *et al.*, 1998; Kurz *et al.*, 2009; Williams and Mukhopadhyay, 2019). The ensuing results yield mixing trends between atmospheric and mantle end members. Nonetheless, this method does not entirely remove the air component. The laser ablation technique pioneered by Burnard (1999) and Burnard *et al.* (1997) to analyse single bubbles, in combination with X-ray microtomography, allowed identifying vesicles connected to the surface by microfractures thereby avoiding analysing air contaminated bubbles (Raquin *et al.*, 2008; Péron *et al.*, 2016). Nevertheless, the possibility of isotopic fractionation during rapid vesiculation (*e.g.*, disequilibrium vesiculation; Aubaud *et al.*, 2004; Ruzié and Moreira, 2010) remains. The highest neon

1. ISTO, CNRS-Université d'Orléans-BRGM, 1a rue de la Férollerie, 45071, Orléans, France
* Corresponding author (email: elena.nunez@etu.univ-orleans.fr)

isotopic compositions measured by step crushing have typically been assumed to have minimal air contamination, providing a lower limit for the mantle (*e.g.*, Yokochi and Marty, 2004; Williams and Mukhopadhyay, 2019). However, the issue is compounded by the possible isotopic fractionation of neon during transport and degassing processes.

In basalt melts CO_2 is the main driver of volatile exsolution. Because CO_2 diffusion is slower than Ne (*e.g.*, Lux, 1987; Nowak *et al.*, 2004), early formed bubbles will get enriched in Ne. Additionally, it is assumed that lighter isotopes such as ^{20}Ne diffuse faster than heavier ones (^{22}Ne), a result of their contrasting molecular weights. This kinetic fractionation during disequilibrium degassing can elevate the $^{20}Ne/^{22}Ne$ ratios in the vesicles. However, this mechanism has not yet been experimentally tested.

This work aims, therefore, to provide such a test by analysing the neon isotopic composition of single vesicles in three experimental samples produced under controlled temperature and pressure conditions.

Materials and Methods

Since CO_2 forms the major gas in the vesicles of the submarine basalt samples from the Atlantic and Pacific (Moore *et al.*, 1977), and we are interested in the isotopic evolution of neon during magma nucleation and vesiculation, the main experimental variables for this study are the duration of the experiment and the amount of CO_2 introduced. Two types of experiments were conducted: (i) CO_2 only experiments, and (ii) CO_2 and Ne-bearing experiments. CO_2-rich experiments served to define the best conditions for producing bubble-rich glass (Fig. S-3), which was then used for the second type of experiments, the main focus of this study. The process of targeting vesicles (of only a few tens of microns; Fig. S-4b,c) amenable to laser ablation is indeed inherently time consuming, and it often requires days or weeks to locate a single vesicle.

For Ne-bearing experiments, the starting material was a basaltic glass previously doped in Ne, mixed with a Ne-free glass of the same composition in a wt. % ratio 1/10 (Supplementary Information and Table S-1). The Ne-doped glass was first prepared by melting the basaltic glass at 1400 °C under a continuous flow of pure Ne at 1 bar for 240 min; this glass was found to have a homogeneous distribution of air-like neon isotopic composition ($^{20}Ne/^{22}Ne = 9.81 \pm 0.01$ and $^{21}Ne/^{22}Ne = 0.0287 \pm 0.0001$; Tables S-2, S-3). The neon solubility of the glass was determined to be $3.16 \pm 0.38 \cdot 10^{-4}$ ccSTP $\cdot$ g^{-1} $\cdot$bar^{-1}.

CO_2 was introduced into the capsule in the form of solid $Ag_2C_2O_4$. During the experiment, the silver oxalate melted, releasing CO_2 as a gas. The amount of CO_2 used in each experiment varied (from 0.17 to 4.49 mg; 0.3–7.2 wt. %) being always enough to saturate the melt with CO_2 under the experimental P and T conditions. This approach enabled bubble nucleation and their upward transport within the capsule. Experiments were performed at pressures between 1535 and 2000 bars and 1200 °C, using sealed $Au_{80}Pd_{20}$ capsules, in an internally heated pressure vessel equipped with a drop quench system (see Supplementary Information for additional details). The duration of the experiments varied from 10 min up to 1800 min, the latter duration approaching equilibrium conditions with respect to CO_2 solubility (Pichavant *et al.*, 2018). Upon quenching, most recovered quenched glasses contained bubbles that were variably distributed across the samples. As shown below, in the longest run (1800 minutes), CO_2 solubility was achieved, and no vesicles were observed in the glass, having fully accumulated on the top of the capsules (sample *EN-E3*). Our procedure simulates the recharge of a degassed (*i.e.* CO_2 and neon-poor) shallow magmatic chamber under isothermal conditions by a melt rich in both CO_2 and neon.

The CO_2 content of quenched glasses was analysed by Fourier-Transform Infrared Spectroscopy (FTIR) (Table S-6). X-ray microtomography was used to characterise each experimental sample's vesicularity and localise the vesicles for laser ablation (Supplementary Information and Tables S-9, S-10 and Fig. S-3). The neon isotopic composition was analysed by coupling laser ablation and mass spectrometry (Table S-8).

Ne Fractionation during Vesiculation

A total of 26 experiments were conducted. Sixteen experiments, in which CO_2 was the sole volatile added, were aimed at examining the evolution of vesicularity over time. The largest average bubble diameter was 38 µm (*ESFa-5B-10min*), while the laser beam diameter was 35 µm, making bubble piercing challenging. Although microtomography helped identify bubble clusters in the samples, single bubble identification during the laser ablation process occurred mostly at random. Based on textural analyses, three out of ten experiments with neon and CO_2 were considered as the most promising and selected for subsequent analyses by mass spectrometry to explore neon isotopic fractionation.

Combining the textural data obtained by microtomography (vesicularity, mean diameter and the vesicle size distribution of each sample; Table S-9 and Fig. S-2) and the results from FTIR (Table S-6), a dynamic interplay is observed between bubble migration; B_d (which is influenced by the rate of bubble growth; G_r) and CO_2 diffusion within the melt; D_{CO2}. Figure 1 shows that during the first 240 min of our experiments, the D_{CO2}, and bubble growth, G_r, are more efficient than the vertical transport of bubbles, B_d, (Fig. 1). In contrast, after 240 min, the average bubble size is large enough for buoyancy to prevail over CO_2 diffusion.

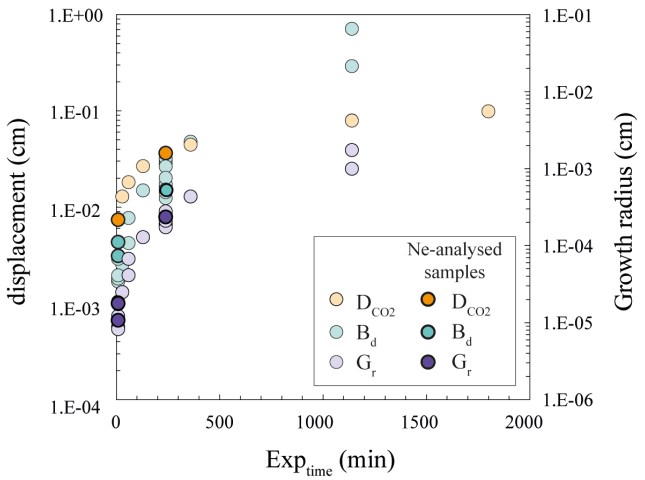

Figure 1 Comparison between CO_2 diffusion in the melt (D_{CO_2}; represented by orange dots) and the displacement of CO_2 bubbles toward the top of the capsule (B_d; represented by blue dots) which depends on bubble radius (G_r, purple dots). Each dot illustrates the state of these three parameters at the time the experiments were quenched. D_{CO2} and B_d are plotted on the left axis, while G_r is on the right, both using logarithmic scales for clarity. Intense colours highlight samples analysed for neon isotopic composition. Details on parameter calculations are provided in the Supplementary Information.

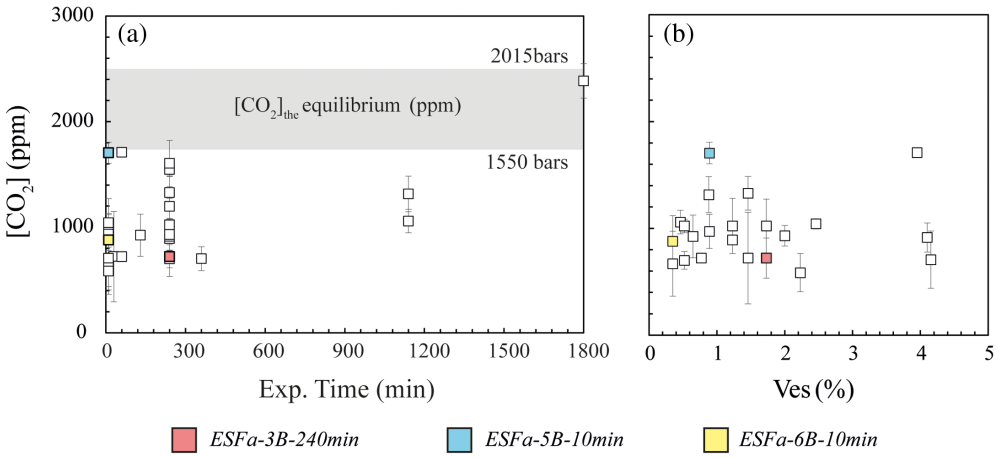

Figure 2 **(a)** Dissolved CO_2 over time and **(b)** comparison with the measured vesicularity of every experimental sample. The grey area points out the maximum CO_2 dissolved expected in the samples for the composition of the magma and the experiment conditions (1200 °C and 1.5–2 kbars; Jiménez-Mejías *et al.* (2021)). The samples analysed for neon isotope compositions are marked following the colour code used in the three neon isotope plot of Figure 3.

The results from FTIR analysis are plotted in Figure 2. The amount of CO_2 added to the experimental capsules had no effect on the dissolved CO_2 (Fig. 2a) or the final vesicularity (Fig. 2b) in samples quenched at the same experimental time. All samples, with the exception of *EN-E3*, plot outside equilibrium conditions (grey field), as shown by the heterogeneous CO_2 content of the glasses, which ranges from 585 up to 1710 ppm (Table S-6), varying by up to 50 % in different points of the same charge. In contrast, the glass of the 1800 min run (sample *EN-E3),* is vesicle-free and has a homogeneous CO_2 distribution of 2385 ± 162 ppm, which is the expected solubility value at the run conditions (equilibrium).

The three experimental samples selected for mass spectrometry are: samples *ESFa-5B* and *ESFa-6B,* corresponding to 10 min of experiment, and sample *ESFa-3B*, which was quenched at the time before the average distance travelled by the vesicles and the diffusion of CO_2 through the melt coincide in time, *i.e.* 240 min (Fig. 1 and Table S-10).

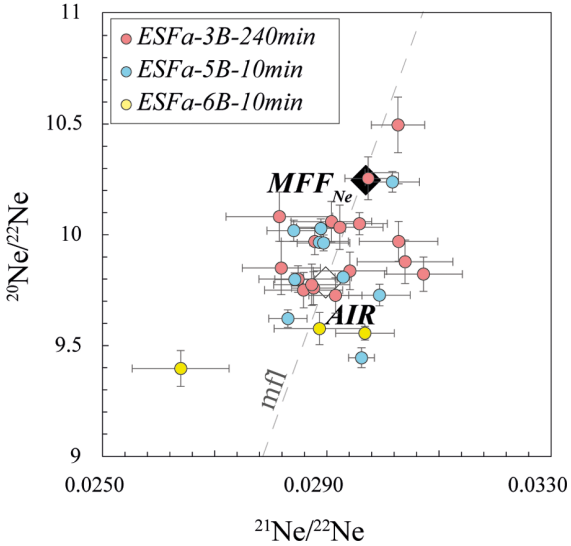

Figure 3 The three neon isotope plot for the vesicles. The black diamond represents the maximum theoretical fractionation factor, MFF_{Ne}, expected for the reference value ($^{20}Ne/^{22}Ne = 10.28$ and $^{21}Ne/^{22}Ne = 0.0297$); the white diamond represents the isotopic ratio of the Ne-bearing starting material ($^{20}Ne/^{22}Ne = 9.81$ and $^{21}Ne/^{22}Ne = 0.0287$). The dashed line represents the mass fractionation line, *mfl*. Data in Table S-8. Uncertainties are 1σ.

Given an air-like starting isotopic composition ($^{20}Ne/^{22}Ne = 9.8$ and $^{21}Ne/^{22}Ne = 0.0290$), the maximum fractionation factor, MFF_{Ne} for the neon isotopes can be estimated from Graham's law, which assumes that the isotopes of neon fractionate during diffusion, in accordance with their mass differences as:

$$MFF_{Ne} = r_{i/j} \cdot (m_j/m_i)^{1/2}$$

where $r_{i/j}$ is the air-like isotopic ratio, m is the mass, and i and j are the light and the heavy isotopes, respectively. This produces $^{20}Ne/^{22}Ne = 10.28$ and $^{21}Ne/^{22}Ne = 0.0297$.

The Ne isotopic compositions from twenty nine out of thirty one vesicles are shown in Figure 3. The plot does not include the vesicles *V2*, and *V9ALA* from sample *ESFa-3B-240min* for which a change of pressure measured during the expansion of the gas in the line after ablation shows that more than one vesicle was pierced (Fig. S-4). The dispersion of the measured Ne isotope ratios along the mass fractionation line suggests that isotopic fractionation occurred to some extent in the three experiments. The $^{20}Ne/^{22}Ne$ isotopic ratios reach values as high as the maximum fractionation factor expected for the initial composition; $V_{2ALA} = 10.50 \pm 0.13$ and $V_{3ALA} = 10.24 \pm 0.05$ for *ESFa-3B-240min* and V4 = 10.24 ± 0.05 for *ESFa-5B-10min* (Table S-8) within 1σ uncertainty. Some of the vesicles show neon isotopic ratios below the air-like starting composition (*e.g.,* V1 = 9.40 ± 0.08 for *ESFa-6B-10min*).

Discussion and Conclusion

This is the first experimental work on neon isotopic fractionation during degassing of a basaltic melt. Figure 4 shows a representative picture of the evolution of our experiments with time.

Figure 4a represents the material loaded in the capsule at time t = 0, before the release of CO_2 by the melting of $Ag_2C_2O_4$ and its subsequent transport through the grains of the basaltic powder. Figure 4b represents an early stage of bubble nucleation in the melt across the capsule. At the onset of the bubble nucleation, driven by CO_2, neon rapidly diffuses into the first nucleated bubbles. As stated previously, due to its higher

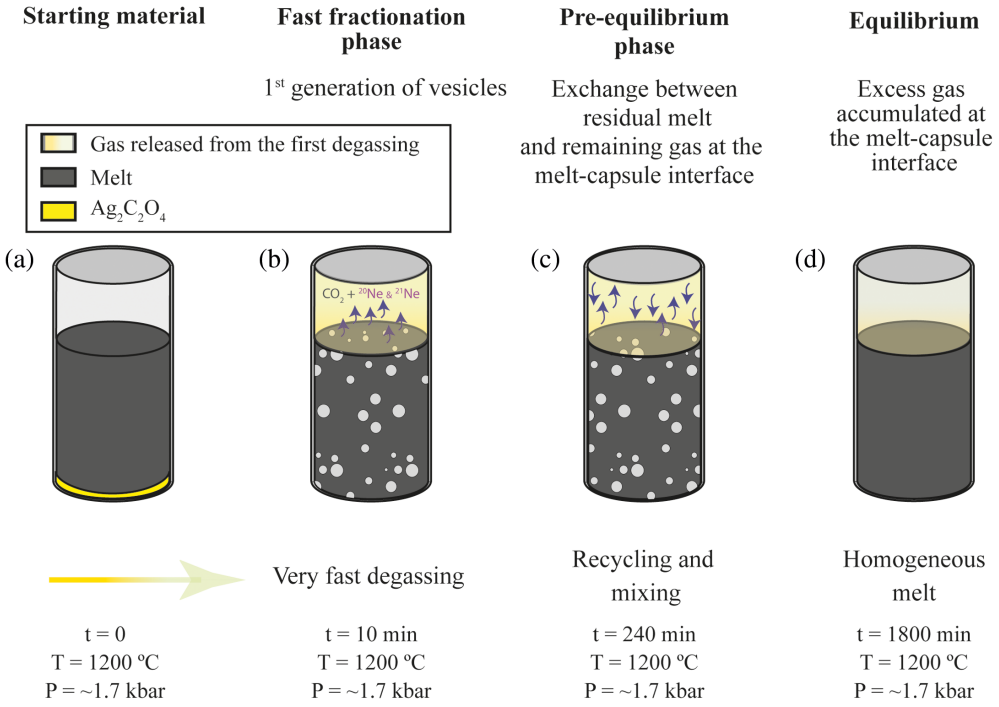

Figure 4 Representative evolution of our experiments from 10 to 1800 minutes. **(a)** The first capsule represents the start of the experiment, with the powdered starting material and the volatile component in the solid phase. The capsules in **(b)** and **(c)** show the experiments at 10 and 240 min. **(d)** shows the final stage of the melt and gas (1800 min, at equilibrium).

diffusivity, neon reaches the vesicles before the CO_2 reaches equilibrium between melt and gas (see Figs. 1, 4b). A significant quantity of gas accumulates at the interface between the melt and the capsule. The gas accumulated at the top of the capsule is presumably rich in ^{20}Ne and ^{21}Ne relative to ^{22}Ne. Correlatively, during this "*fast fractionation phase*" (Fig. 4b), the melt becomes depleted in these light isotopes. This explains the low $^{20}Ne/^{22}Ne$ and $^{21}Ne/^{22}Ne$ isotopic ratios (less than 9.66 and 0.0273 respectively, including the scatter error) observed in vesicles V_{10} and V_{11} in sample *ESFa-5B-10min* and the three analysed vesicles of sample *ESFa-6B-10min*. Unfortunately, the gas accumulated at the capsule-glass interface after quenching could not be analysed.

During the experiment, the gas trapped at the melt-capsule interface continuously interacts with the melt (Fig. 4c). Meanwhile, bubbles grow either through inward diffusion of CO_2 (since the pressure remains stable during the experiment, vesicles cannot grow by gas expansion) or through bubble coalescence and strive to reach isotopic equilibrium. This is the case for all of the analysed vesicles with air-like $^{20}Ne/^{22}Ne$ and $^{21}Ne/^{22}Ne$ isotopic ratios, mostly belonging to sample *ESFa-3B-240min* (Table S-8). However, newly formed bubbles (vesicles that continue to nucleate) are fractionated, and at this time, as the melt is interacting also with the gas accumulated at the capsule-melt interface (with high isotopic ratios as explained previously), and the resultant new vesicles have $^{20}Ne/^{22}Ne$ and $^{21}Ne/^{22}Ne$ isotopic ratios as high as 10.50 and 0.0303 respectively (vesicle V_2; Table S-8). Different generations of vesicles can be observed while the experiments last longer, with new nuclei of vesicles and vesicles with larger sizes compared to those formed in shorter experiments (Fig. S-2). As the duration of the experiments increases (from 10 to 1140 minutes), there is a noticeable decrease in the number of smaller vesicles (which correspond to the nuclei of new bubbles), an increase in the vesicle mean diameter, along with the accumulation of vesicles at the top capsule-melt interface, until the main body of melt is vesicle-free and the gas phase at the top of the capsule reaches equilibrium with the melt. The latter case is illustrated by the sample *EN-E3*, which lacks bubbles, and in which the measured dissolved CO_2 content is 2385 ± 162 ppm (Fig. 4d), in good agreement with the solubility determined by Jiménez-Mejías *et al.* (2021) (2487 ppm) for the conditions of the experiment, indicating attainment of equilibrium.

The results of our experiments demonstrate that in a system in which bubbles are continuously nucleating (*i.e.* while the system is oversaturated in CO_2) the last formed vesicles will tend to be kinetically fractionated until the diffusion of all isotopes of Ne reaches equilibrium. The same phenomenon can be expected to occur with other noble gases, as for example argon.

The principal implication of this work bears on the interpretation of the analyses of the gas trapped in magma vesicles in natural samples. Our findings suggest that when a CO_2-rich magma enters a reservoir, the resident magma might be unable to assimilate this new flux if degassing occurs too fast. This is due to the contrasted diffusivities of the various volatile species (here CO_2 and Ne) and of the different isotopes involved, producing a mass dependent isotope fractionation. Consequently, caution must be exercised when interpreting the highest values obtained from the analysis of noble gases in bubbles of natural samples (either by crushing extraction or by laser ablation of single vesicles), as faithfully recording the isotopic composition of the mantle source, in particular whenever fast degassing processes are suspected. While this work represents a critical step for identifying the source of neon in the Earth's mantle, for the time being it does not definitively favour any of the proposed scenarios. Yet, it shows that isotopic fractionation due to mass dependence could account for the high values observed in some natural samples, suggesting that the dissolution of the solar nebula in a magma ocean is not the only possible explanation.

Acknowledgements

The authors acknowledge support from LabEx VOLTAIRE (ANR-10LABX-100-01) and the European Research Council (ERC) (Grant agreement No.101096688[APATE][ERC-2022-ADG]). We are grateful to J. Andujar, I. Di Carlo, A. Slodczyk and P. Penhoud for their help during experiments and analyses as well as to the anonymous reviewers for their constructive comments.

Editor: Romain Tartèse

Additional Information

Supplementary Information accompanies this letter at https://www.geochemicalperspectivesletters.org/article2505.

Cite this letter as: Núñez-Guerrero, E., Moreira, M., Scaillet, B. (2025) Isotopic fractionation of neon during magma degassing. *Geochem. Persp. Let.* 34, 1–5. https://doi.org/10.7185/geochemlet.2505

References

Aubaud, C., Pineau, F., Jambon, A., Javoy, M. (2004) Kinetic disequilibrium of C, He, Ar and carbon isotopes during degassing of mid-ocean ridge basalts. *Earth Planetary Science Letters* 222, 391–406. https://doi.org/10.1016/j.epsl.2004.03.001

Ballentine, C.J., Marty, B., Sherwood Lollar, B., Cassidy, M. (2005) Neon isotopes constrain convection and volatile origin in the Earth's mantle. *Nature* 433, 33–38. https://doi.org/10.1038/nature03182

Black, D.C. (1972) On the origins of trapped helium, neon and argon isotopic variations in meteorites—II. Carbonaceous meteorites. *Geochimica Cosmochimica Acta* 36, 377–394. https://doi.org/10.1016/0016-7037(72)90029-4

Burnard, P. (1999) The bubble-by-bubble volatile evolution of two mid-ocean ridge basalts. *Earth Planetary Science Letters* 174, 199–211. https://doi.org/10.1016/S0012-821X(99)00254-X

Burnard, P., Graham, D., Turner, G. (1997) Vesicle-specific noble gas analyses of "popping rock": implications for primordial noble gases in Earth. *Science* 276, 568–571. https://doi.org/10.1126/science.276.5312.568

Colin, A., Moreira, M., Gautheron, C., Burnard, P. (2015) Constraints on the noble gas composition of the deep mantle by bubble-by-bubble analysis of a volcanic glass sample from Iceland. *Chemical Geology* 417, 173–183. https://doi.org/10.1016/j.chemgeo.2015.09.020

Eberhardt, P., Geiss, J., Graf, H., Grögler, N., Mendia, M., Mörgeli, M., Schwaller, H., Stettler, A., Krähenbühl, U., Von Gunten, H. (1972) Trapped solar wind noble gases in Apollo 12 lunar fines 12001 and Apollo 11 breccia 10046. *Proceedings of the Third Lunar Science Conference, Supplement 3, Geochemical et Cosmochemical Acta, The MIT press 2*, 1821–1856.

Harper Jr, C.L., Jacobsen, S.B. (1996) Noble gases and Earth's accretion. *Science* 273, 1814–1818. https://doi.org/10.1126/science.273.5283.1814

Heber, V.S., Baur, H., Bochsler, P., McKeegan, K.D., Neugebauer, M., Reisenfeld, D.B., Wieler, R., Wiens, R.C. (2012) Isotopic mass fractionation of solar wind: Evidence from fast and slow solar wind collected by the Genesis mission. *Astrophysics Journal* 759, 121. https://doi.org/10.1088/0004-637X/759/2/121

Honda, M., McDougall, I., Patterson, D.B., Doulgeris, A., Clague, D.A. (1993) Noble gases in submarine pillow basalt glasses from Loihi and Kilauea, Hawaii: a solar component in the Earth. *Geochimica Cosmochimica Acta* 57, 859–874. https://doi.org/10.1016/0016-7037(93)90174-U

Jiménez-Mejías, M., Andújar, J., Scaillet, B., Casillas, R. (2021) Experimental determination of H2O and CO2 solubilities of mafic alkaline magmas from Canary Islands. *Comptes Rendus Géoscience* 353, 289–314. https://doi.org/10.5802/crgeos.84

Kurz, M.D., Curtice, J., Fornari, D., Geist, D., Moreira, M. (2009) Primitive neon from the center of the Galápagos hotspot. *Earth Planetary Science Letters* 286, 23–34. https://doi.org/10.1016/j.epsl.2009.06.008

Lux, G. (1987) The behavior of noble gases in silicate liquids: Solution, diffusion, bubbles and surface effects, with applications to natural samples. *Geochimica. Cosmochimica Acta* 51, 1549–1560. https://doi.org/10.1016/0016-7037(87)90336-X

Mizuno, H., Nakazawa, K., Hayashi, C. (1980) Dissolution of the primordial rare gases into the molten Earth's material. *Earth Planetary Science Letters* 50, 202–210. https://doi.org/10.1016/0012-821X(80)90131-4

Moore, J.G., Batchelder, J.N., Cunningham, C.G. (1977) CO_2-filled vesicles in mid-ocean basalt. *Journal of Volcanology and Geothermal Research*, 2, 309–327. https://doi.org/10.1016/0377-0273(77)90018-X

Moreira, M., Kunz, J., Allegre, C. (1998) Rare gas systematics in popping rock: isotopic and elemental compositions in the upper mantle. *Science* 279, 1178–1181. https://doi.org/10.1126/science.279.5354.1178

Moreira, M., Charnoz, S. (2016) The origin of the neon isotopes in chondrites and on Earth. *Earth Planetary Science Letters* 433, 249–256. https://doi.org/10.1016/j.epsl.2015.11.002

Mukhopadhyay, S. (2012) Early differentiation and volatile accretion recorded in deep-mantle neon and xenon. *Nature* 486, 101–104. https://doi.org/10.1038/nature11141

Nowak, M., Schreen, D., Spickenbom, K. (2004) Argon and CO_2 on the race track in silicate melts: a tool for the development of a CO_2 speciation and diffusion model. *Geochimica Cosmochimica Acta* 68, 5127–5138. https://doi.org/10.1016/j.gca.2004.06.002

Péron, S., Moreira, M., Colin, A., Arbaret, L., Putlitz, B., Kurz, M.D. (2016) Neon isotopic composition of the mantle constrained by single vesicle analyses. *Earth Planetary Science Letters* 449, 145–154. https://doi.org/10.1016/j.epsl.2016.05.052

Péron, S., Moreira, M., Putlitz, B., Kurz, M. (2017) Solar wind implantation supplied light volatiles during the first stage of Earth accretion. *Geochemical Perspectives Letters* 3, 151–159. https://doi.org/10.7185/geochemlet.1718

Péron, S., Moreira, M., Agranier, A. (2018) Origin of light noble gases (He, Ne, and Ar) on Earth: A review. *Geochem. Geophysics Geosystems* 19, 979–996. https://doi.org/10.1002/2017GC007388

Pichavant, M., Le Gall, N., Scaillet, B. (2018) Gases as precursory signals: experimental simulations, new concepts and models of magma degassing. In: Gottsmann, J., Neuberg, J., Scheu, B. (Eds.) *Volcanic Unrest. From Science to Society*. Springer, 139–154. https://doi.org/10.1007/11157_2018_35.

Raquin, A., Moreira, M.A., Guillon, F. (2008) He, Ne and Ar systematics in single vesicles: mantle isotopic ratios and origin of the air component in basaltic glasses. *Earth Planetary Science Letters*. 274, 142–150. https://doi.org/10.1016/j.epsl.2008.07.007

Raquin, A., Moreira, M. (2009) Atmospheric $^{38}Ar/^{36}Ar$ in the mantle: implications for the nature of the terrestrial parent bodies. *Earth Planetary Science Letters* 287, 551–558. https://doi.org/10.1016/j.epsl.2009.09.003

Ruzié, L., Moreira, M. (2010) Magma degassing process during Plinian eruptions. *Journal of Volcanology and Geothermal Research* 192, 142–150. https://doi.org/10.1016/j.jvolgeores.2010.02.018

Trieloff, M., Kunz, J., Clague, D.A., Harrison, D., Allègre, C.J. (2000) The Nature of Pristine Noble Gases in Mantle Plumes. *Science* 288, 1036–1038. https://doi.org/10.1126/science.288.5468.1036

Williams, C.D., Mukhopadhyay, S. (2019) Capture of nebular gases during Earth's accretion is preserved in deep-mantle neon. *Nature* 565, 78–81. https://doi.org/10.1038/s41586-018-0771-1

Yatsevich, I., Honda, M. (1997) Production of nucleogenic neon in the Earth from natural radioactive decay. *Journal of Geophysical Research Solid Earth* 102, 10291–10298. https://doi.org/10.1029/97JB00395

Yokochi, R., Marty, B. (2004) A determination of the neon isotopic composition of the deep mantle. *Earth and Planetary Science Letters* 225, 77–88. https://doi.org/10.1016/j.epsl.2004.06.010